Lung Cancer 217 (2026) 109354

Contents lists available at ScienceDirect

Lung Cancer

journal homepage: www.elsevier.com/locate/lungcan

Research Paper

MORPHEUS-Lung: biomarkers and clinical response to atezolizumab + bevacizumab + stereotactic body radiotherapy in patients with metastatic non-small cell lung cancer

Byoung Chul Cho [a,1], Sun Min Lim [b,1], Sang Hoon Lee [c,d,1], Dong Kwon Kim [d,e,1], Nuria Pardo [f], Hen Prizant [g,*], Yaacov R. Lawrence [h], Nedal Al-Sakaff [i], Hans-Joachim Helms [i], Velimir Gayevskiy [g,j], Barzin Y. Nabet [g], Jan Pintoffl [i], Francois Ghiringhelli [k]

[a] Yonsei Cancer Center, Yonsei University College of Medicine, Seoul, South Korea
[b] Division of Medical Oncology, Department of Internal Medicine, Yonsei University College of Medicine, Seoul, South Korea
[c] Yonsei New II Han Institute for Integrative Lung Cancer Research, Yonsei University College of Medicine, Seoul, South Korea
[d] Severance Biomedical Science Institute, Yonsei University College of Medicine, Seoul, South Korea
[e] Brain Korea 21 PLUS Project for Medical Science, Yonsei University College of Medicine, Seoul, South Korea
[f] Vall d'Hebron University Hospital, Vall d'Hebron Institute of Oncology (VHIO), Barcelona, Spain
[g] Genentech, Inc., South San Francisco, CA, USA
[h] The Benjamin Davidai Dep. Radiation Oncology Sheba Medical Center affiliated with Tel Aviv University, Tel-Hashomer, Ramat-Gan, Israel
[i] F. Hoffmann-La Roche Ltd, Basel, Switzerland
[j] Rancho BioSciences, San Diego, CA, USA
[k] Department of Medical Oncology, Centre le Cancer G.-F. Leclerc, INSERM, Université Bourgogne Europe, Dijon, France

ARTICLE INFO

Keywords:
Non-small cell lung cancer
RNA sequence analysis
MORPHEUS
Immune checkpoint inhibitors
Radiotherapy

ABSTRACT

Introduction: Results from the MORPHEUS-Lung (NCT03337698) study suggest that atezolizumab + bevacizumab + stereotactic body radiotherapy (SBRT) was associated with numerically improved efficacy outcomes vs docetaxel (control) in immune checkpoint inhibitor–exposed patients with metastatic non-small cell lung cancer. We report exploratory analyses to identify potential biomarkers associated with this clinical response.
Methods: Tumor samples were analyzed for differential gene expression and pathway/immune subset gene signatures by single cell RNA-sequencing and further validated with bulk RNA-sequencing.
Results: The biomarker-evaluable population included 58 patients from two cohorts (atezolizumab + bevacizumab + SBRT, n = 26; docetaxel [control], n = 32). In a discovery study, analyses of clinical benefit (CB) vs non-CB groups at baseline showed that resident-memory CD8 T cells (T_{RM}) were significantly enriched (P = 0.027; Gini index: P = 0.018), and expression of CXCL10$^+$ and FOLR2$^+$ macrophages was increased in the CB group. Pre- and post-treatment analysis showed that expression of effector-memory CD45RA$^+$ CD8 T cells (T_{EMRA}), CD8 T_{RM}, and FOLR2$^+$ and FABP4$^+$ macrophages were numerically increased post-treatment. Together these results led to the identification of curated T-cell– and macrophage-associated gene response signatures. Using a confirmatory cohort, gene signature expression aligned with survival outcomes for patients receiving atezolizumab + bevacizumab + SBRT.
Conclusions: These results suggest that activation of T cells and macrophages are associated with a favorable clinical response to atezolizumab + bevacizumab + SBRT. Moreover, CD8 T_{RM}, CD8 exhausted T cells, and CXCL10$^+$ macrophages may serve as potential biomarkers of response to atezolizumab + bevacizumab + SBRT treatment and potentially aid in tailored, precision medicine for individual patients.

* Corresponding author at: Genentech Research & Early Development, Genentech, Inc., 1 DNA Way, South San Francisco, CA 94080, USA.
E-mail address: prizanthen@gene.com (H. Prizant).
[1] B.C. Cho, S.M. Lim, S.H. Lee, and D.K. Kim contributed equally as co-first authors.

https://doi.org/10.1016/j.lungcan.2026.109354
Received 10 December 2025; Received in revised form 26 February 2026; Accepted 1 March 2026
Available online 7 May 2026

1. Introduction

Globally, non-small cell lung cancer (NSCLC) accounts for approximately 85% of all lung cancers [1]. Five-year survival rates for metastatic disease are 14.3% [2]. The use of immune checkpoint inhibitors (CPIs) such as programmed cell death protein-1 (PD-1)/PD-ligand 1 (PD-L1) antibodies has revolutionized the treatment landscape for metastatic NSCLC (mNSCLC). In the second-line setting, treatment options for patients with mNSCLC are largely dependent on the first-line treatment received [3]. Currently approved second-line therapies include pemetrexed, docetaxel, nivolumab, atezolizumab, and pembrolizumab in patients with mNSCLC without targetable driver mutations or rearrangements [3]. However, given the relatively poor prognosis still seen for CPI-exposed patients [4], there is a need for additional treatment options, including combination therapies with a CPI.

MORPHEUS-Lung (NCT03337698) is a signal-seeking, global, Phase Ib/II, open-label, multicenter, randomized, umbrella study in patients with mNSCLC, focusing on quickly assessing combinations with atezolizumab (anti-PD-L1) vs a control arm given docetaxel, which is considered a standard-of-care treatment for CPI-exposed patients with non-squamous histology [5]. Combination therapies evaluated in this study included (but were not limited to) atezolizumab + bevacizumab + immune-modulating non-ablative stereotactic body radiotherapy (SBRT) and atezolizumab + bevacizumab [5]. Bevacizumab, a monoclonal antibody that binds to vascular endothelial growth factor A (VEGF-A), promotes the normalization of tumor vasculature and can thereby increase the access of therapeutic agents [6]. Moreover, bevacizumab has demonstrated immunomodulatory properties [7] and has shown clinical efficacy in combination with atezolizumab in several tumor types [8–10]. Radiotherapy transforms irradiated tumors into *in situ* vaccinations through the induction of tumor antigen release and the activation of T-cell–mediated immune responses [11,12]. When used in combination with a CPI, radiotherapy modulates the immunesuppressive tumor stromal microenvironment and augments the effects of CPIs, while CPIs counteract the immunosuppressive effects of radiotherapy through the amplification of the radiation-induced abscopal effect [13,14]. Moreover, in the PEMBRO-RT study, SBRT + pembrolizumab demonstrated improved response rates and survival outcomes vs pembrolizumab alone in patients with PD-L1 negative mNSCLC [15]. At the interim analysis, atezolizumab + bevacizumab with or without SBRT showed evidence of numerically improved progression-free survival (PFS; atezolizumab + bevacizumab + SBRT [7.7 months; 95% CI: 4.4, 11.4] or atezolizumab + bevacizumab [7.0 months; 95% CI: 4.4, 8.3]) vs docetaxel (4.8 months; 95% CI: 4.1, 6.4) and numerically improved overall survival (OS; atezolizumab + bevacizumab + SBRT [16.9 months; 95% CI: 9.76, not evaluable] or atezolizumab + bevacizumab [13.7 months; 95% CI: 10.6, 21.1]) vs docetaxel (11.0 months; 95% CI: 8.34, 18.60). Therefore, these combinations may represent a potential chemotherapy-free treatment option for patients with mNSCLC [5].

Given the number of CPIs and potential combinations available, predictive biomarkers are needed to help identify patients who are more likely to benefit from different therapeutic options [16]. PD-L1 is the only U.S. Food and Drug Administration–approved biomarker in NSCLC for predicting response to CPIs; however, PD-L1 is limited by tumor heterogeneity and detection variability [17]. T-cell receptor (TCR) clonality, spatial distribution, phenotypic diversity, and functional states of tumor-infiltrating lymphocytes (TILs), and exhaustion markers such as *PDCD1*, which encodes PD-1, are emerging novel biomarkers that might play a role in predicting response to CPIs [18].

At the interim analysis, no clear correlations between response and PD-L1 expression or immune phenotype were seen in the MORPHEUS-Lung study [5]. However, it was noted that patients with PD-L1–negative and immune desert tumors derived benefit from atezolizumab + bevacizumab + SBRT [5]. Therefore, we report additional exploratory analyses from the MORPHEUS-Lung study in CPI-exposed patients with mNSCLC to identify potential biomarkers associated with clinical response to atezolizumab + bevacizumab + SBRT.

2. Materials and methods

2.1. Study design and patient population

The MORPHEUS-Lung study design was previously reported [5]. Briefly, eligible patients were those that experienced disease progression during or following treatment with a platinum-containing regimen and an anti-PD-L1/PD-1 CPI, given in combination as one line of therapy or as two separate lines of therapy, regardless of PD-L1 expression. Patients were randomized to the atezolizumab + bevacizumab + SBRT, atezolizumab + bevacizumab, or docetaxel control arms.

A 1200 mg intravenous (IV) infusion of atezolizumab was administered on Day 1 of each 21-day cycle until unacceptable toxicity or loss of clinical benefit occurred. A 15 mg/kg IV infusion of bevacizumab was administered on Day 1 of each 21-day cycle until unacceptable toxicity or loss of clinical benefit occurred. A 75 mg/m^2 IV dose of docetaxel was administered over 60 min on Day 1 of each 21-day cycle.

SBRT was administered prior to atezolizumab + bevacizumab, and three fractions of 8 Gy were completed within 21 days (±5 days) after receiving consent and within 7 days of initiating atezolizumab + bevacizumab. Only photon (x-ray) beams with photon energies of at least 6 MV were allowed. Patients that entered the SBRT arm may have had any number of active lesions. One to five lesions of 1 to 5 cm diameters located anywhere in the body outside of the brain could be irradiated. Target sites and lesion types for each patient in the biomarker analysis are shown in Supplementary Table S1. Lesions abutting organs at risk and sensitive to radiation and lesions treated with SBRT within the last 6 months were not irradiated.

Patients were classified based on clinical outcomes following treatment with atezolizumab + bevacizumab + SBRT or docetaxel. Clinical benefit (CB) was defined as those patients who exhibited a complete response (CR), partial response (PR), or stable disease (SD) with PFS $\geq$ 6 months. Non-CB (NCB) was defined as those patients with progressive disease (PD) or SD with PFS $<$ 6 months.

The study was done in conformance with Good Clinical Practice guidelines and the Declaration Helsinki. The protocol was reviewed and approved by the institutional review board or ethics committee at each study site. All amendments affecting trial recruitment and conduct were approved. All patients provided written, informed consent.

2.2. Single-cell RNA sequencing (scRNA-seq) analyses

In the initial discovery study, scRNA-seq was used to analyze differentially expressed gene (DEG) and pathway/immune subset gene signatures between the CB and NCB groups and the pre- and post-treatment sample from the atezolizumab + bevacizumab + SBRT arm only. Fresh tumor tissue samples, required for single-cell analysis were collected by biopsy at study entry (five patients) and 6 weeks post-treatment (one patient). The analytical framework used to identify these gene signatures in T cells and macrophages included clustering using Uniform Manifold Approximation and Projection (UMAP), gene set enrichment analysis (GSEA) of DEGs, clonal expansion using the Gini index, trajectory analyses using Monocle3, and intercellular communication between different cell types using CellChat. Full details of the RNA-seq procedures are provided in the Supplementary Methods.

2.3. Bulk RNA-seq analyses

In the secondary confirmatory study, bulk RNA-seq was conducted on samples from both the atezolizumab + bevacizumab + SBRT and docetaxel control arms of the biomarker-evaluable population (BEP) to validate T-cell– and macrophage-associated gene signatures identified during scRNA-seq analyses. Baseline formalin-fixed paraffin-embedded

(FFPE) tumor tissue samples were collected from all patients, preferably by biopsy performed at study entry. Where a biopsy was not deemed feasible by the investigator, archival tumor tissue was used, provided the patient had not received any immune CPI therapy since the time of the biopsy. T-cell– and macrophage-associated gene signatures were validated by survival outcomes in the CB and NCB groups and stratified by treatment arms. Full details of the bulk RNA-seq procedures are provided in the Supplementary Methods.

2.4. Statistical analysis

All statistical analyses conducted in this study were exploratory with no alpha adjustment for multiple testing performed and were completed using R (v4.4.2). Continuous variables were compared between two groups using either the Wilcoxon rank sum-test or Student's *t*-test, as appropriate. Associations between categorical variables across two or more groups were evaluated using the X^2 test. Statistical significance was defined as $P < 0.05$ for all statistical tests. Survival analyses were conducted using Cox-proportional hazard models. Full details of the statistical analyses are provided in the Supplementary Methods.

2.5. Data availability

The data sets generated or analyzed during the current study are available from the corresponding author upon reasonable request.

3. Results

3.1. Study population

The overall BEP was comprised of the patients for whom FFPE tumor tissue samples were obtained (n = 58). Twenty-six of these patients received atezolizumab + bevacizumab + SBRT and 32 received docetaxel (Supplementary Table S2). We conducted integrated analyses using scRNA-seq from five patients as an initial discovery study and bulk RNA-seq (n = 58) as a secondary confirmatory study to identify potential biomarkers associated with clinical efficacy to atezolizumab + bevacizumab + SBRT.

In the initial discovery study, four of the five patients with fresh baseline tumor tissue samples were from the CB group and one was from the NCB group (Supplementary Table S3). In total, six baseline samples (four from four patients in the CB group and two from one patient in the NCB group) from tumor tissue biopsies were analyzed. Additionally, a post-treatment fresh tumor tissue biopsy was collected from one patient in the CB group following treatment with atezolizumab + bevacizumab + SBRT.

In the secondary confirmatory study, 26 of the 58 patients with samples received atezolizumab + bevacizumab + SBRT and 32 received docetaxel. Fifty-three patients had confirmed best overall response and were not censored. Out of these 53 patients, 26 were from the CB group and 27 were from the NCB group. In the CB group, 14 patients received atezolizumab + bevacizumab + SBRT and 12 received docetaxel; in the NCB group, 11 patients received atezolizumab + bevacizumab + SBRT and 16 received docetaxel.

3.2. Phenotypic distribution of T/natural killer (NK) cells within the tumor microenvironment (TME) of mNSCLC in the CB and NCB groups

Potential biomarkers were identified from the analysis of the six pre-treatment samples. scRNA sequencing data from 11,646 single cells were subjected to unsupervised clustering, revealing seven distinct cell populations. Among these, T/NK cells accounted for 64% of the total cell population, while myeloid cells comprised 7.4% (Supplementary Fig. S1A, B).

First, we explored the T/NK cell subsets within the TME through the annotation of CD4 T cells, CD8 T cells, and NK cells (Fig. 1A). Notably, *PDCD1* was highly expressed in CD4 CXCL13, CD8 exhausted T cells (T_{EX}), and interferon (IFN)-activating CD8 T cells (Supplementary Fig. S1C). Interestingly, CD8 T_{EX} cells showed a transcriptional profile comparable to IFN-activating CD8 T cells, with elevated expression of IFN-γ, NK markers, and lytic granules-mediated cytotoxic markers seen (Supplementary Fig. S1D).

Next, we examined the relative abundance of CD4 and CD8 T cells by response to atezolizumab + bevacizumab + SBRT treatment. Resident-memory CD8 T cells (T_{RM}) and CD8 central memory T cells (T_{CM}) were significantly enriched in the CB vs the NCB groups (mean value: CB, 4.5% vs NCB, 2.0%; $P = 0.027$, and mean value: CB, 13.0% vs NCB, 4.8%; $P = 0.046$, respectively) (Fig. 1B). Furthermore, effector-memory CD45RA+ CD8 T cells (T_{EMRA}) exhibited a trend toward higher abundance in the NCB group compared with the CB group. DEG analysis of CD8 T cells in the CB group revealed upregulation of *PDCD1*, *LAG3*, and *TIGIT*, as well as genes associated with T-cell activation (*CXCR4*) and inflammatory responses (*TNFAIP3*, *NFKBIA*; Fig. 1C). Further elucidating the molecular programs associated with treatment response, GSEAs of the CB and NCB group DEGs in CD8 T cells showed that the CB group exhibited enrichment of pathways related to T-cell activation, type II IFN production, and peptide antigen assembly (Fig. 1D).

To investigate if CD8 T-cell subsets were associated with treatment response, we calculated the Gini index. Our analysis showed that intratumoral CD8 T cells have a similar level of clonal expansion regardless of type of T cell. Notably, the Gini index of tumor-infiltrating CD8 T_{RM} was significantly higher in the CB group than in the NCB group (mean value: CB, 30.0% vs NCB, 18.0%; $P = 0.018$; Fig. 1E).

3.3. Intratumoral differentiation trajectory analysis of CD8 T cells in the CB and NCB groups

Monocle3 analysis revealed that the trajectory originating from CD8 T_{CM} branched into three distinct pathways leading to CD8 T_{EMRA}, CD8 T_{RM}, and CD8 T_{EX} (Fig. 2A). Notably, in the CB group, there was a higher spatial distribution of T_{RM} and CD8 T_{EX}, whereas the NCB group showed relatively higher localization of CD8 effector memory T cells (T_{EM}) and CD8 T_{EMRA} (Fig. 2B). To further assess lineage-specific changes, we performed a trajectory analysis. CD8 T_{EM} was set as the root of the trajectory, as its relative abundance between CB and NCB groups was most similar (Supplementary Fig. S1E). Comparison of the density of CD8 T cells across the three lineages revealed distinct differences between the CB and NCB groups. In the differentiation trajectory towards CD8 T_{EX}, the CB group showed a progressive accumulation of CD8 T_{EX} cells over virtual time, while NCB exhibited a pattern of stasis at early stages.

In the CD8 T_{EMRA} lineage, the cell density at the terminal end of the trajectory was higher in the NCB group than in the CB group. Clonality was overall higher at the terminal end of the trajectory in the CB group than in the NCB group (Fig. 2C). Finally, in the CD8 T_{RM} lineage, there was a trend of increased CD8 T_{RM} density as virtual time progressed in the CB group when compared with the NCB group.

When comparing gene expression between the final differentiation states of CD8 T_{EMRA} from the NCB group samples and CD8 T_{RM} and CD8 T_{EX} from the CB group samples, the results showed that pathways related to T-cell activation and differentiation were significantly enriched in CD8 T_{RM} compared with CD8 T_{EMRA} (Fig. 2D). Additionally, CD8 T_{EX} showed a markedly enriched activation of immune cell activation and antigen presentation pathways compared with CD8 T_{EMRA} (Fig. 2E, Supplementary Table S4). GSEA analysis comparing biological pathways between the CB and NCB groups showed that despite the lower abundance of T_{EMRA} cells in the CB group, T-cell–related functional pathways were enriched (Supplementary Fig. S1F).

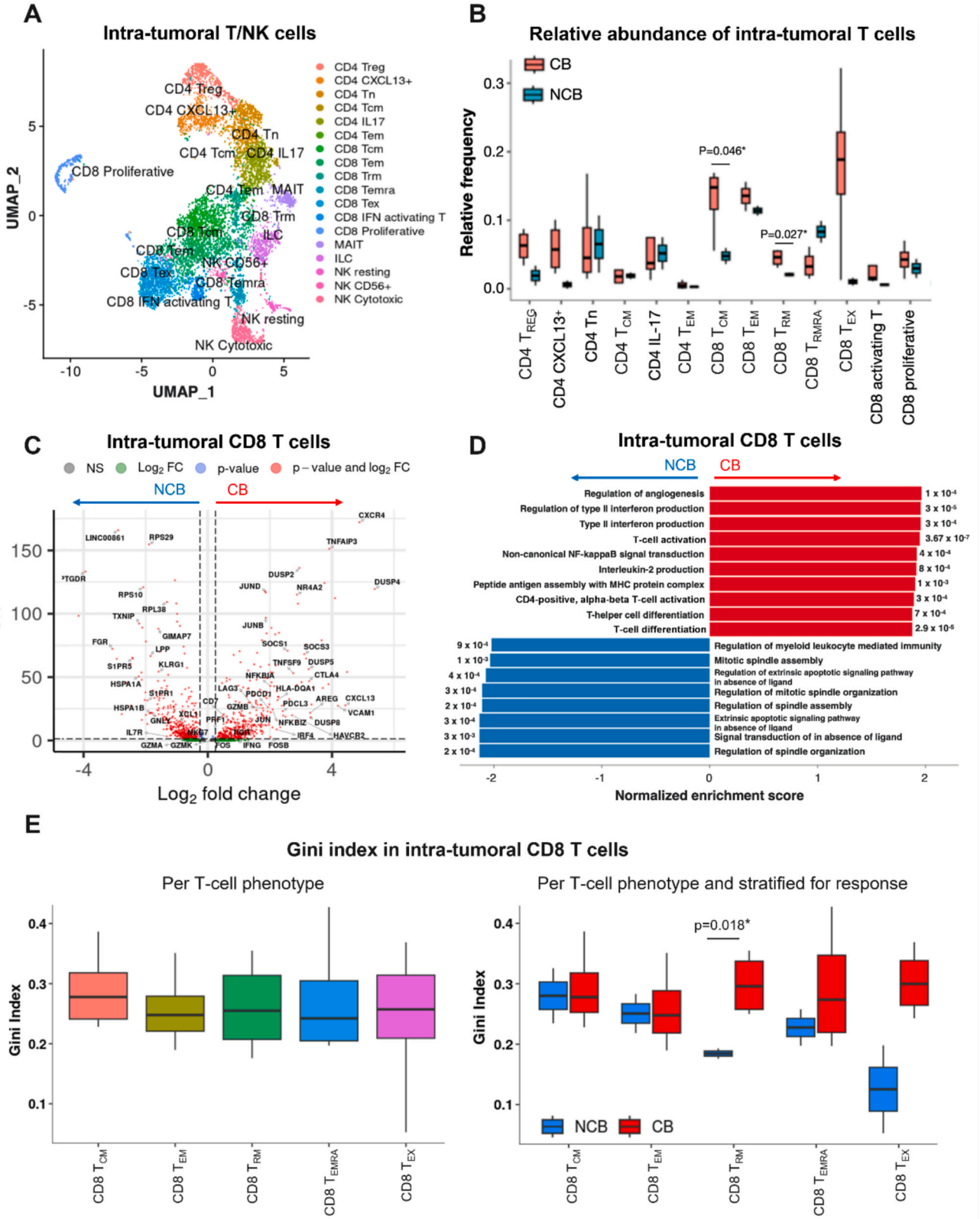

(caption on next page)

Fig. 1. Phenotypic distribution of T/NK cell subsets in the TME of mNSCLC in the CB and NCB groups. **A,** UMAP representation depicting intratumoral T/NK-cell phenotypes (n = 6). **B,** Boxplots depicting relative abundance of intratumoral T/NK-cell phenotypes calculated per tumor samples and stratified for response (CB and NCB). *P*-values calculated using *t*-test; only *P*-values < 0.05 are shown. Boxes plus whiskers indicate the median ± IQR. The whiskers extend from either the first or third quartile to 1.5 × IQR. **C,** Volcano plot depicting differentially expressed genes in intratumoral CD8 T cells (n = 3,930) from CB samples (n = 4; 3,575 CD8 T cells) vs NCB samples (n = 2; 355 CD8 T cells. *P*-values were obtained using the Wilcoxon test and Bonferroni corrected. Red: adjusted *P*-value < 0.05 and $\log_2$-fold change > 0.25). **D,** Biological pathways comparing CB (PR + SD) and NCB (PD). **E,** Gini-index of intratumoral CD8 T cells. Left: calculated per samples (n = 6), per CD8 T-cell phenotype. Right: calculated per sample (n = 6) and stratified per response (4 CB and 2 NCB). *P*-values calculated using *t*-test; only *P*-values < 0.05 are shown. Boxes plus whiskers indicate the median ± IQR. The whiskers extend from either the first or third quartile to 1.5 × IQR. CB, clinical benefit; CXCL, C-X-C motif chemokine ligand; NCB, non-clinical benefit; NK, natural killer; PD, progressive disease; PR, partial response; SD, stable disease; T_{CM}, CD8 central memory T cell; T_{EMRA}, effector-memory CD45RA + CD8 T cell; T_{EM}, effector memory T cell; T_{EX}, exhausted T cell; T_{reg}, regulatory T cell; T_{RM}, tissue-resident memory T cell; UMAP, uniformed manifold approximation and projection. (For interpretation of the references to colour in this figure legend, the reader is referred to the web version of this article.)

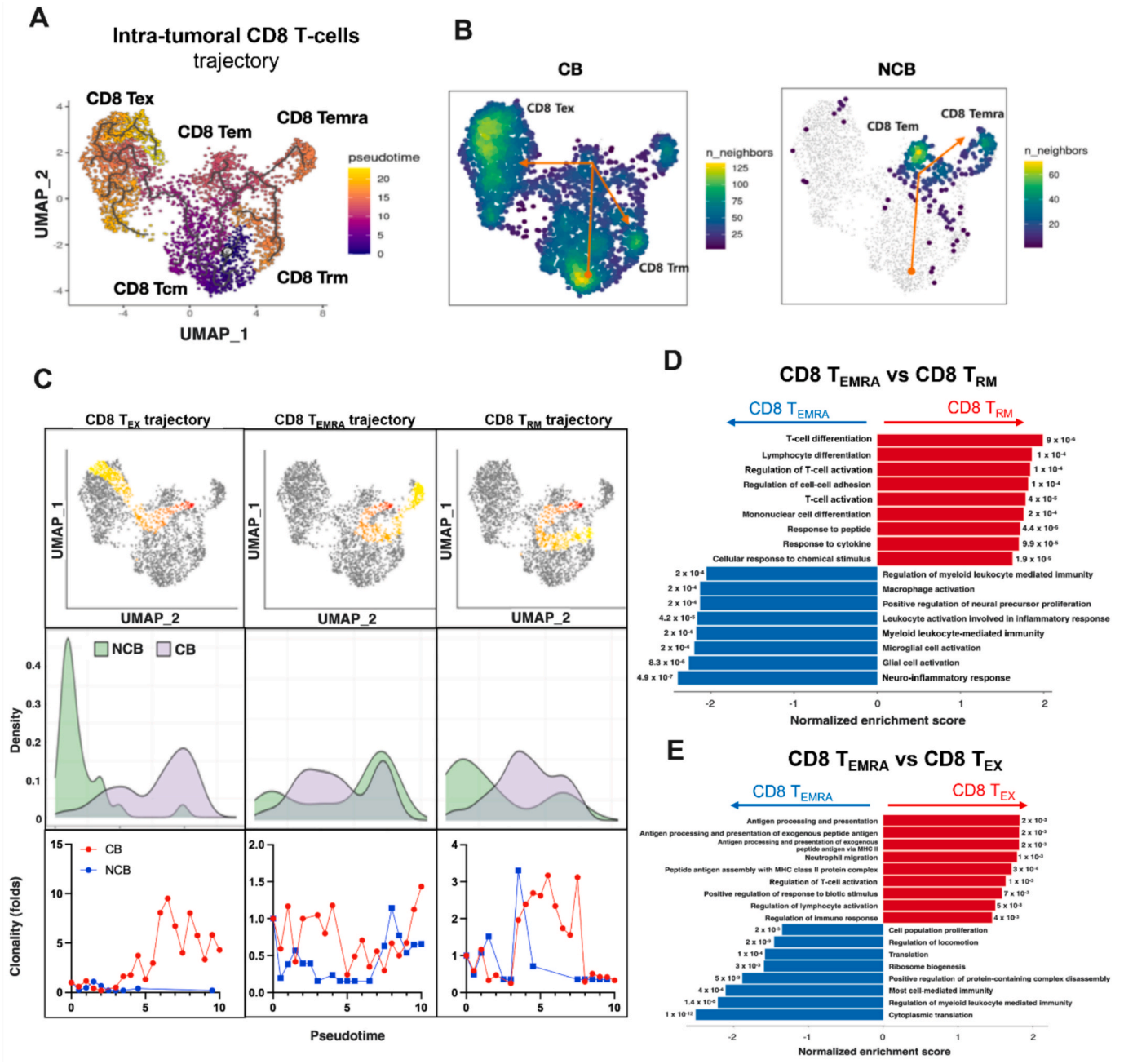

Fig. 2. Trajectory analysis of CD8 T-cell subtypes in the CB and NCB groups. **A,** Depicting trajectory direction by pseudotime. **B,** Trajectory direction on CB and NCB. **C,** T cell density, TCR clonality along with CD8 trajectory in atezo + bev + SBRT–treated samples (n = 6), stratified for response (n = 4 for CB and n = 2 for NCB). **D,** Biological pathways comparing CD8 T_{EMRA} vs CD8 T_{RM}. *P*-value < 0.05 and $\log_2$ fold change > 0.1. **E,** Biological pathways comparing CD8 T_{EMRA} vs CD8 T_{EX}. *P*-value < 0.05 and $\log_2$ fold change > 0.1. atezo, atezolizumab; bev, bevacizumab; CB, clinical benefit; CD, cell determinant; NCB, non-clinical benefit; TCR, T-cell receptor; T_{EMRA}, effector-memory CD45RA + CD8 T cell; T_{EX}, exhausted T cell; T_{RM}, tissue-resident memory T cell.

3.4. Phenotypic distribution of PD-L1–expressing cells within the TME in the CB and NCB groups

Within the monocyte/macrophage compartment of PD-L1–expressing myeloid-derived cells, we identified various tumor-associated macrophage (TAM) subtypes using marker genes. Notably, we identified CXCL10^{+} macrophages, which exhibited high expression of genes involved in T cell recruitment, such as *CXCL9*, *CXCL10*, and *CXCL11* (Fig. 3A. Supplementary Fig. S2A). Comparison of the relative abundance of TAM subtypes between the CB and NCB groups revealed that CXCL10^{+} macrophages and folate receptor beta^{+} (FOLR2^{+}) macrophages appeared more abundant in the CB group, while secreted phosphoprotein 1^{+} (SPP1^{+}) macrophages and triggering receptor expressed on myeloid cells 2^{+} (TREM2^{+}) macrophages appeared more abundant in the NCB group, although these differences were not statistically significant (Supplementary Fig. S2B). DEG analysis showed that genes related to T cell recruitment (*CXCL9*, *CXCL10*, *CXCL11*) and immune cell migration and inflammation regulation (*CCL8*, *CCL13*) were highly expressed in the CB group, whereas the expression of immunosuppressive genes (*CD5L*, *CD52*) was increased in the NCB group (Fig. 3B). Importantly, the expression of *CD274*, which encodes the therapeutic target PD-L1, was higher in myeloid-derived cells from

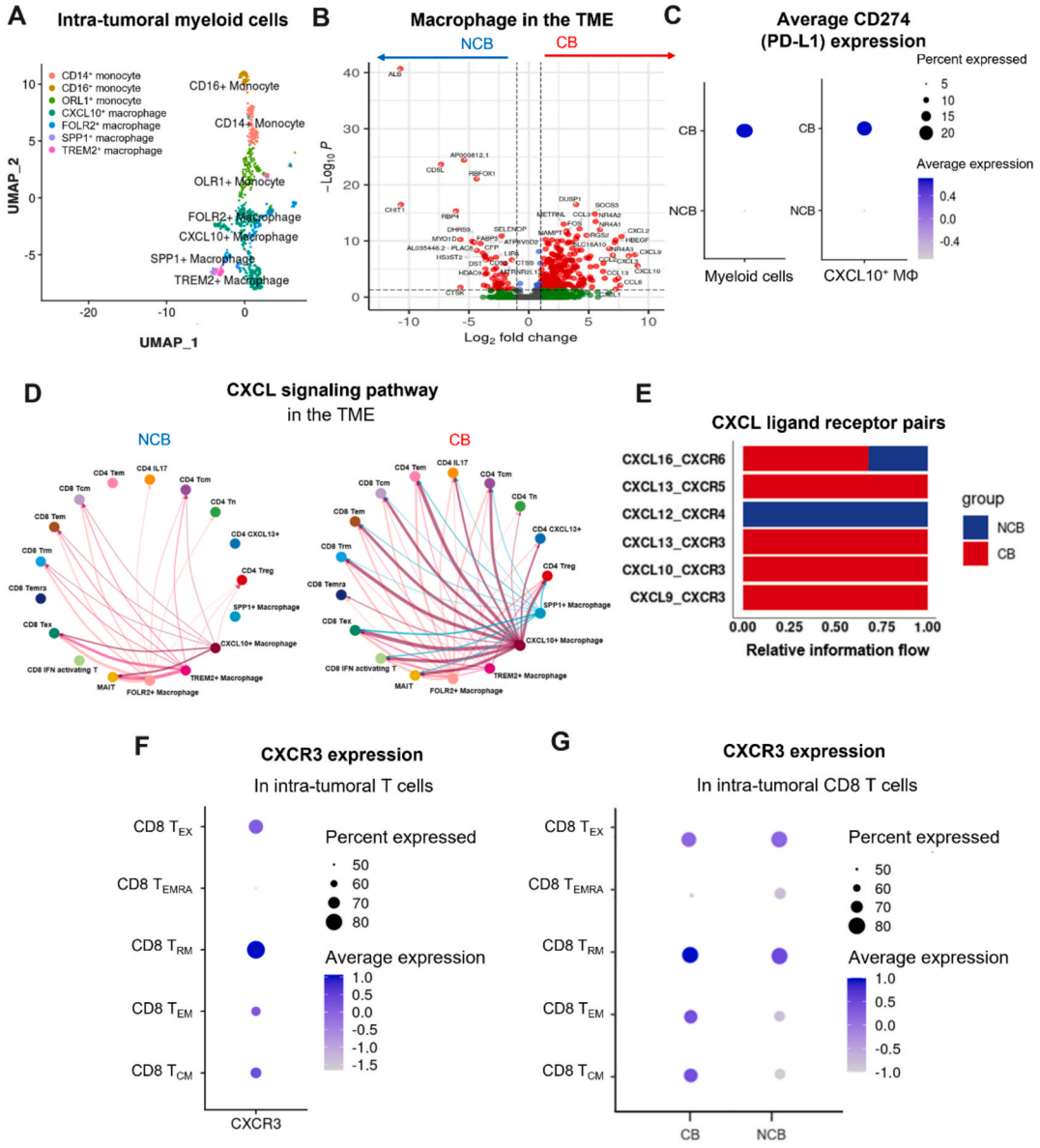

Fig. 3. Phenotypic distribution of monocytes and macrophages in the TME of mNSCLC in the CB and NCB groups. **A,** UMAP representation of monocyte and macrophage phenotypes in the TME. **B,** Volcano plot of differentially expressed genes in macrophages (n = 563) in the TME of the CB group (n = 4) vs the NCB group (n = 2). *P*-values were obtained using the Wilcoxon test and Bonferroni-corrected. Red: adjusted *P*-value < 0.05 and $\log_2$ fold change > 0.25. **C,** Dot plot depicting the mean expression levels of *CD274* (PD-L1) in CB and NCB within bone marrow cells (left; n = 6; n = 4 in the CB group and n = 2 in the NCB group), and within CXCL10^{+} macrophages (right; n = 6; n = 4 in the CB group and n = 2 in the NCB group). **D,** Circos plot of the CXCL signaling pathway in the TME, depicting cell–cell interactions between intratumoral macrophages (sender) and intratumoral T cells (receiver) in the CB group (left) and NCB group (right). **E,** Bar plot depicting the overall information flow for each ligand receptor pair of the CXCL signaling pathway in the TME of the CB vs NCB groups. Overall information flow is defined by the sum of the communication probability among all pairs of cell groups in the inferred network. *P*-value calculated using Wilcoxon test (only *P*-values < 0.05 are shown). **F,** Dot plot of *CXCR3* expression in intratumoral CD8 T cells. **G,** Dot plot of *CXCR3* expression in the CB and NCB groups. CB, clinical benefit; CXCL, C-X-C motif chemokine ligand; NCB, non-clinical benefit; TME, tumor microenvironment; UMAP, uniformed manifold approximation and projection. (For interpretation of the references to colour in this figure legend, the reader is referred to the web version of this article.)

the CB group than the NCB group (Fig. 3C, **left**). More specifically, *CD274* expression was highest in CXCL10$^+$ macrophages (Supplementary Fig. S2C), and CXCL10$^+$ macrophages showed higher levels of *CD274* expression in the CB group (Fig. 3C, **right**).

Next, we explored how CXCL10$^+$ macrophages in the TME express T-cell recruitment genes and interact with T cells. Analysis of significant immune cell interactions between the CB and NCB groups revealed that, overall, more interactions were observed in the CB group (Supplementary Fig. S2D). Focusing on the CXCL signaling pathway, we found that, compared with the NCB group, the predicted interactions between CXCL10$^+$ macrophages and T cells were more abundant in the CB group (Fig. 3D). Analysis of ligand-receptor pairs revealed that the *CXCL16-CXCR6* ligand interaction was significantly increased in both the CB and NCB groups; the *CXCL12-CXCR4* ligand interaction was significantly increased in the NCB group; and *CXCL9-CXCR3*, *CXCL10-CXCR3*, *CXCL13-CXCR3*, and *CXCL13-CXCR5* ligand-receptor interactions were significantly increased in the CB group compared with the NCB group ($P < 0.05$; Fig. 3E). Notably, the expression of *CXCR3* was highest in the CD8 T_{RM} subtype of CD8 T cells, and expression was also detected in CD8 T_{EX}, CD8 T_{EM}, and CD8 T_{CM} cells (Fig. 3F). Furthermore, in the CB group, not only CD8 T_{RM} but also CD8 T_{EM} and CD8 T_{CM} exhibited higher *CXCR3* expression compared with the NCB group (Fig. 3G).

3.5. Phenotypic distribution of T/NK cells in the TME of the pre- and post-treatment samples

To investigate treatment-induced alterations in the TME, we applied the same analytical framework to perform a detailed characterization of the T/NK cell compartment in the paired biopsy sample from a single patient. Sub-clustering of tumor-infiltrating T cells and NK cells revealed distinct phenotypic subtypes for CD4 and CD8 T cells, as well as independent phenotypic subsets for NK cells (Supplementary Fig. S3A, B). Gene expression analysis of the CD8 T cells in the post-treatment sample (Post) revealed upregulation of a CD8 T_{RM} marker (*ZNF683*), CD8 T_{EMRA} marker *SPON2*, and *IFNG*. In contrast, the pre-treatment sample (Pre) exhibited increased expression of immune checkpoint genes *LAG3*, *HAVCR2*, and *CXCL13* (Fig. 4A).

An assessment of functional pathways associated with DEGs between the Pre and Post samples in CD8 T cells was conducted. DEGs in Pre and Post samples showed upregulation of pathways related to hypoxia response, radiation response, and leukocyte differentiation in the Post sample (Fig. 4B). To evaluate the effects of radiation therapy, we compared the gene set scores of genes included in previously identified radiation response-related pathways (Supplementary Table S3). The analysis revealed an increase in gene set scores in the Post vs Pre samples, with particularly high values seen in the CD8 T_{RM} and CD8 T_{EMRA} cell types (Fig. 4C).

Analysis of TCR expansion for each T-cell phenotype showed that prior to treatment with atezolizumab + bevacizumab + SBRT, the predominant T-cell clones within the tumor were primarily found in the 'antigen-experienced' T-cell clusters, particularly in CD8 T_{EX}. However, after treatment, these dominant clones were predominantly seen in CD8 T_{EMRA} and CD8 T_{RM} (Fig. 4D). Interestingly, when examining cytotoxic markers within CD8 T-cell subsets, high expression of cytotoxic markers was observed in both CD8 T_{EMRA} and CD8 T_{RM} (Fig. 4E).

When examining the origins of CD8 T_{RM} and CD8 T_{EMRA} in the TME, analyses revealed that the trajectory originating from the CD8 T_{CM} branched into three distinct paths leading to CD8 T_{EMRA}, CD8 T_{RM}, and CD8 T_{EX} (Supplementary Fig. S3C). Notably, in the Pre sample, differentiation through CD8 T_{EM} into CD8 T_{EX} was dominant, whereas in the Post sample, differentiation through CD8 T_{EM} into CD8 T_{RM} and CD8 T_{EMRA} was prominent (Fig. 4F). When considering CD8 T_{CM} as the origin of the trajectory, we observed differences in CD8 T cell density between the Pre and Post samples across all three lineages (Fig. 4G). In the lineage leading to CD8 T_{EX}, the Pre sample showed a tendency for increased T cell density toward the end of the trajectory compared with the Post sample. In contrast, in the differentiation pathways leading to CD8 T_{EMRA} and CD8 T_{RM}, the Post sample exhibited higher T cell density at the end of the trajectory compared with the Pre sample. In the differentiation pathway leading to CD8 T_{EMRA}, the T cell density in the Pre sample decreased with psuedotime, whereas the Pre sample T cell density appeared to remain consistent in the differentiation leading to CD8 T_{RM}.

We hypothesized that the immunological activity of CD8 T_{EMRA} cells may be further amplified by radiation therapy. Consistent with this, DEEG analysis between Pre and Post samples revealed that T-cell activation and T-cell differentiation pathways were numerically increased in CD8 T_{EMRA} cells in the Post sample compared with the Pre sample (Supplementary Fig. S3D).

3.6. Phenotypic distribution of macrophage T-cell phenotypes within the TME in the pre- and post-treatment samples

We then investigated changes in the TME before and after treatment. These analyses revealed the emergence of fatty acid binding protein 4$^+$ (FABP4$^+$) macrophages after treatment (Fig. 5A). DEG analysis of TAMs showed that the expression of *CXCL9* and *CXCL10* were higher in the Pre sample, which corresponds with the sample being derived from the CB group, whereas the marker gene *FABP4* was highly enriched in the Post sample (Fig. 5B).

The emergence of FABP4$^+$ macrophages in the Post sample appears to be attributed to the metabolic effects of bevacizumab. DEG analysis between FABP4$^+$ macrophages and other macrophage subsets showed that pathways related to fatty acid metabolism were significantly enriched in FABP4$^+$ macrophages (Supplementary Fig. S4A). Biological function analysis of the four macrophage subsets showed that CXCL10$^+$ macrophages were associated with enhanced innate immunity, while FOLR2$^+$ macrophages showed increased functions related to T cell activation and differentiation (Supplementary Fig. S4B). Furthermore, analysis of *CD274* expression in macrophage subsets showed a significant increase in expression levels in TREM2$^+$ macrophages and FABP4$^+$ macrophages in the Post sample (Supplementary Fig. S4C).

Trajectory analysis of tumor-infiltrating macrophages in the TME revealed that macrophage differentiation starts from CD14$^+$ monocytes and progresses to FOLR2$^+$ macrophages and FABP4$^+$ macrophages (Fig. 5C). Interestingly, macrophages from the Pre and Post samples exhibited divergent differentiation patterns. In the Pre sample, the trajectory was restricted to CXCL10$^+$ macrophages, whereas in the Post sample, further differentiation occurred from CXCL10$^+$ macrophages to FOLR2$^+$ macrophages, and TREM2$^+$ macrophages tended to differentiate into FABP4$^+$ macrophages (Fig. 5D).

Assessment of the radiation response score of macrophages revealed that it was higher in the Post sample than in the Pre sample (Supplementary Fig. S4D). Furthermore, within the Post sample, FOLR2$^+$ macrophages exhibited the highest radiation response, suggesting that FOLR2$^+$ macrophages differentiated from CXCL10$^+$ macrophages in response to radiation therapy.

Intercellular interaction analysis between FOLR2$^+$ and FABP4$^+$ macrophages and T cells in the Post sample showed that FOLR2$^+$ macrophages were found to primarily interact with T cells through the inducible T-cell costimulatory (ICOS) signaling pathway (Fig. 5E). Moreover, the *ICOSLG* expressed on FOLR2$^+$ macrophages exhibited the highest interaction with *ICOS* on T cells and was also shown to interact with *CTLA4* (Supplementary Fig. S4E). Among the macrophage subtypes in the Post sample, expression of *ICOSLG* was most prominently observed in FOLR2$^+$ macrophages. *ICOS* was highly expressed in CD8 T_{RM}, CD8 T_{CM}, CD8 T_{EM}, and CD8 T_{EX} cells, whereas *CTLA4* exhibited the highest expression in CD8 T_{EX} cells (Fig. 5F). Additionally, analysis of CD4 T cell subtypes revealed that *CTLA4* was highly expressed in CD4 regulatory T (T_{reg}) cells, contributing to immune suppression (Supplementary Fig. S4G, left).

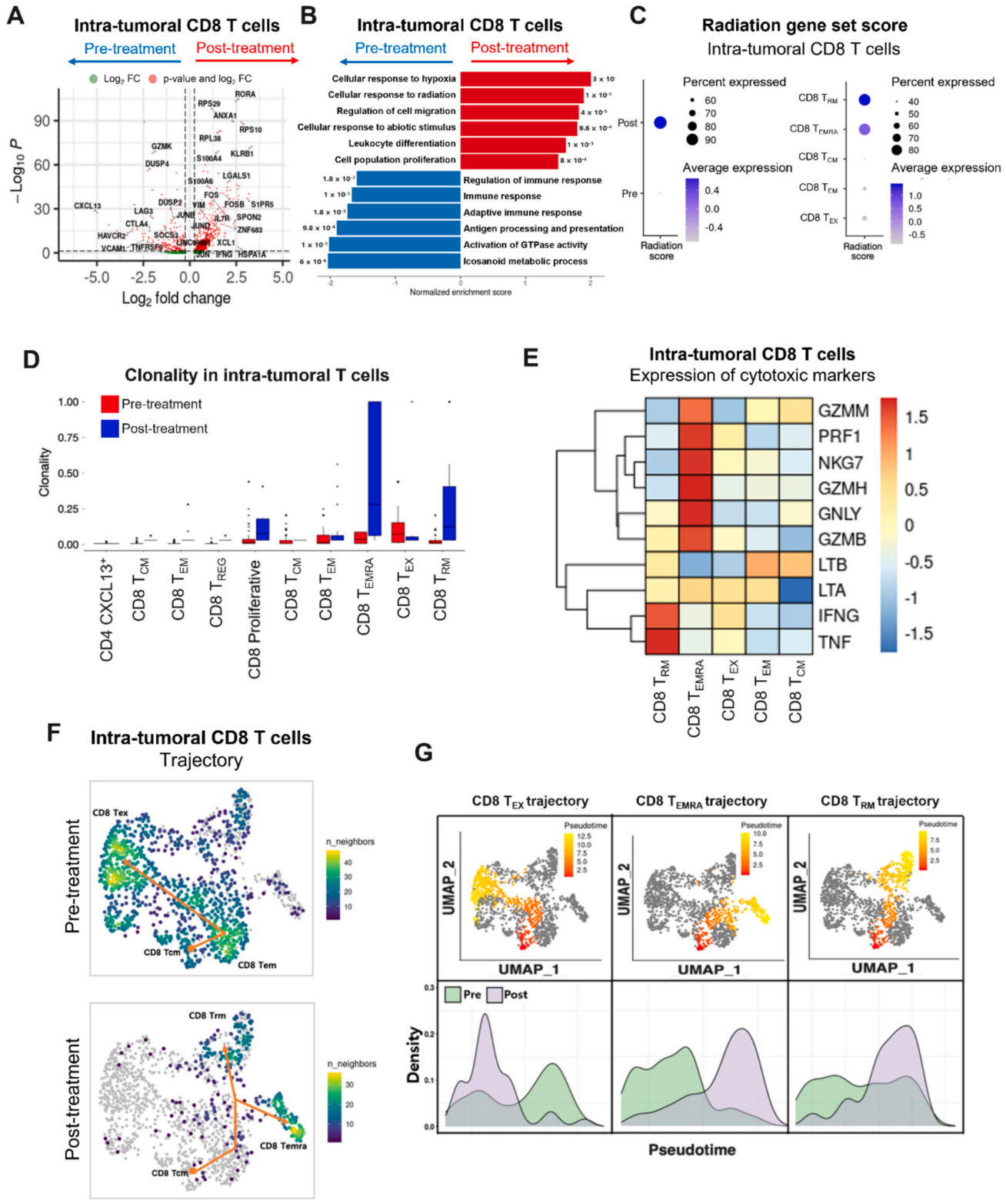

Fig. 4. Differential gene expression analysis in the pre- and post-treatment samples. **A,** Volcano plot depicting differentially expressed genes in intratumoral CD8 T cells (two samples, n = 1,483 CD8 T cells) from Post sample (one sample, n = 299 CD8 T cells) vs Pre sample (one sample, n = 1,184 CD8 T cells). *P*-values were obtained using the Wilcoxon test and Bonferroni corrected. Red; adjusted *P*-value < 0.05 and $\log_2$ fold change > 0.25. **B,** Biological pathways comparing Pre and Post samples. **C,** The expression of genes associated with radiation response. Left: Dot plot of radiation gene set score in intratumoral CD8 T cells (Pre and Post). Right: Dot plot of radiation gene set score in intratumoral CD8 T cells (Pre and Post). **D,** Clonality of intratumoral T cells. **E,** Heatmaps showing expression of cytotoxic genes in intratumoral CD8 T cells. **F,** Trajectory direction on the CB and NCB groups. **G,** T cell density, each CD8 trajectory in atezo + bev + SBRT samples (n = 2), stratified for response (one Pre and one Post). The density plots reflect the relative number of T cells separately for Pre vs Post along each CD8 trajectory. atezo, atezolizumab; bev, bevacizimab, CB, clinical benefit; CD, cell determinant; NCB, non-clinical benefit; Post, post-treatment sample; Pre, pre-treatment sample; SBRT, stereotactic body radiotherapy. (For interpretation of the references to colour in this figure legend, the reader is referred to the web version of this article.)

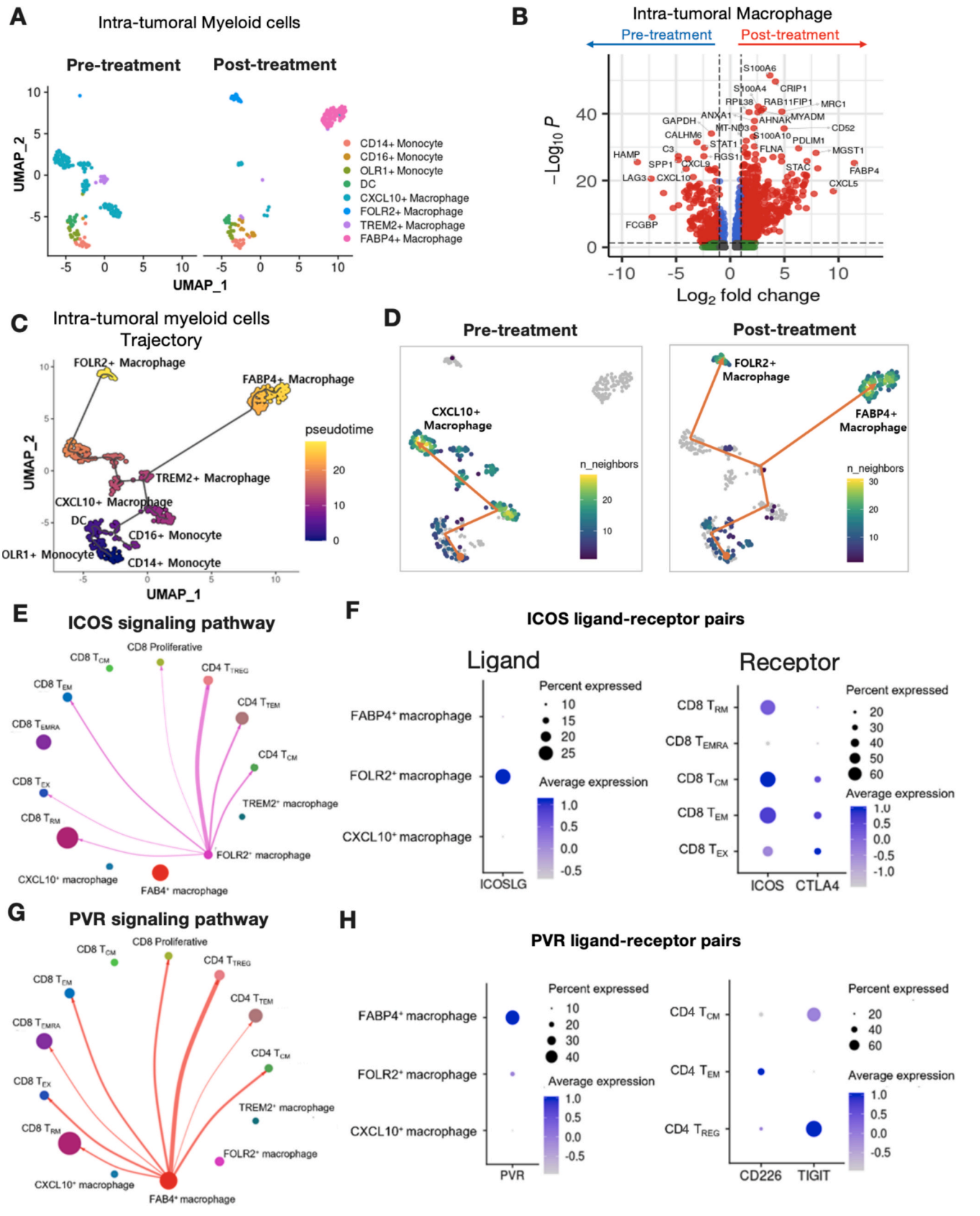

(caption on next page)

Fig. 5. Phenotypic distribution of macrophage T-cell phenotypes in the pre- and post-treatment samples. **A,** The UMAP representation of monocyte and macrophage phenotypes in the Pre (one sample, n = 218 myeloid cells) and Post (one sample, n = 203 myeloid cells) samples. **B,** Volcano plot of differentially expressed genes in macrophages (n = 304 cells) in the TME of the Pre vs Post samples. *P*-values were obtained using Wilcoxon test and Bonferroni-corrected. Red: adjusted *P*-value < 0.05 and $\log_2$ fold change > 0.25. **C,** Depicting trajectory direction by pseudotime. **D,** Trajectory direction in the Pre and Post samples. **E,** Circos plot on the ICOS signaling pathway in the TME, depicting cell–cell interactions between intratumoral macrophages (sender) and intratumoral T cells (receiver) in the Post sample. **F,** The expression of ligand and receptor pairs associated with ICOS signaling. Left: Dot plot of *ICOSLG* expression in intratumoral macrophage cells from the Post sample. Right: Dot plot of *ICOS*, *CTLA4* expression intratumoral CD8 T cells from the Post sample. **G,** Circos plot of the PVR signaling pathway in the TME, depicting cell–cell interactions between intratumoral macrophages (sender) and intratumoral T cells (receiver) in the Post sample. **H,** Expression of ligand and receptor pairs associated with PVR signaling. Left: Dot plot of *CD155* expression, which encodes the PVR ligand, in intratumoral macrophage cells from the Post sample. Right: Dot plot of *CD226*, *TIGIT* expression in intratumoral CD4 T cells from the Post sample. CD, cell determinant; ICOS, inducible T cell costimulatory; Pre, pre-treatment sample; Post, post-treatment sample; PVR, poliovirus receptor; TME, tumor microenvironment; UMAP, uniformed manifold approximation and projection. (For interpretation of the references to colour in this figure legend, the reader is referred to the web version of this article.)

Next, FABP4$^+$ macrophages were found to interact with T cells primarily through the poliovirus receptor (PVR) signaling pathway (Fig. 5G). Additionally, *CD155*, which encodes the PVR ligand expressed on FABP4$^+$ macrophages, showed the strongest interaction with TIGIT on T cells, as well as an interaction with *CD226*, which encodes the DNAX accessory molecule-1 (DNAM-1) receptor (Supplementary Fig. S4F). Among the macrophage subtypes in the Post sample, *CD155* was most prominently expressed on FABP4$^+$ macrophages (Fig. 5H). *CD226* was highly expressed on CD4 T_{EM} cells, whereas *TIGIT*, was highly expressed on CD4 T_{reg} cells and showed lower expression CD4 T_{CM} cells. In CD8 T-cell subtype analysis, *CD226* was highly expressed on CD8 T_{RM} cells, whereas *TIGIT* was highly expressed on CD8 T_{EX} cells, contributing to immune suppression, followed by CD8 T_{EM} cells and CD8 T_{RM} cells (Supplementary Fig. S4G, right).

3.7. Activation of biological pathways in pre- and post-treatment samples

To assess the effects of atezolizumab + bevacizumab + SBRT treatment on epithelial cells, we analyzed the activity of key biological pathways. The angiogenesis and epithelial-mesenchymal transition (EMT) pathway scores, reflecting the effects of bevacizumab, showed a decreased score in the Post sample compared with the Pre sample. Additionally, although the glycolysis score decreased in the Post sample, the fatty acid metabolism score increased. The radiation response score was numerically increased in the Post sample, with notable activation of the tumor growth factor (TGF)-β signaling and p53 pathways in the Post sample compared with the Pre sample (Supplementary Fig. S5).

3.8. Survival outcomes in the CB and NCB groups and stratified by treatment arm

Using scRNA-seq, we analyzed transcriptomic differences between the CB (n = 4) and NCB (n = 2) groups. With DEG analysis, we identified a set of top 10 genes in T cells and macrophages, respectively, that were significantly upregulated in the CB group compared with the NCB group. By conducting gene set scoring, we noted that CB signature in the T-cell (CBST) and CB signature in the macrophage (CBSM) were significantly upregulated in the CB group (Fig. 6A; Supplementary Table S5).

We next validated these T-cell– and macrophage-associated response signatures in a larger study cohort (n = 58) using bulk RNA sequencing. When we compared z-scores within treatment groups (atezolizumab + bevacizumab + SBRT [n = 26] vs docetaxel [n = 32]), both signatures showed a trend toward increased expression in the CB group treated with atezolizumab + bevacizumab + SBRT (Fig. 6**B-C**).

Analysis of survival outcomes showed that patients with high expression of both CBST and CBSM gene signatures showed numerically improved PFS and OS when treated with atezolizumab + bevacizumab + SBRT vs docetaxel, whereas patients with lower expression of these biomarkers showed no significant differences in PFS or OS (Fig. 6**D-G**).

4. Discussion

Although CPI monotherapy and combination treatments have led to improvement in survival outcomes for patients with mNSCLC, not all patients have a durable CB from treatment. Therefore, it is essential that effective biomarkers are identified to differentiate potential responders from non-responders prior to treatment initiation [16]. The TME is a crucial factor that influences the clinical response to CPIs. Numerous studies have identified that TILs play an important role in anti-tumor activity and mediating response to CPIs [19–21]. Hence, evaluating the phenotypic distribution of TILs at diagnosis could be used to predict CPI treatment response. In this study, we used scRNA-seq and bulk RNA-seq analyses of tumor biopsies from CPI-exposed patients with mNSCLC in the MORPHEUS-Lung study to identify potential biomarkers associated with CB from atezolizumab + bevacizumab + SBRT treatment.

Numerous studies have shown that there is a positive correlation between CD8 T cell expression and CPI treatment outcome in several tumor types [21–23]. In particular, these correlations have been seen with CD8 T-cell subsets T_{RM} and T_{EX} [24–27]. Similarly, when we compared the CB group vs the NCB group, our results showed that CD8 T_{RM} cells within the TME may promote response to atezolizumab + bevacizumab + SBRT in mNSCLC and may play a central role in immune responses including inducing anti-tumor immunity activation in the CB group. Furthermore, CD8 T_{EX} cells were closely associated with immune therapy responsiveness. Therefore, the distinct gene expression profiles and immune pathways of CD8 T_{RM} and CD8 T_{EX} may serve as biomarkers for predicting the CB of immune therapy and provide a novel framework for assessing treatment response.

Next, we investigated whether a target for atezolizumab + bevacizumab + SBRT could be found in PD-L1 expressing cells. We found that PD-L1 expressing CXCL10$^+$ macrophages, activated in the TME prior to treatment, were associated with response to atezolizumab + bevacizumab + SBRT therapy. Moreover, tumor antigen–recognizing CD8 T_{RM} cells, which highly express PD-L1, may undergo functional enhancement upon PD-L1 inhibition by atezolizumab through interaction with CXCL10$^+$ macrophages. This promotes the recruitment and activation of CXCR3$^+$ T_{EM} cells leading to immune activation within the TME. Rather than acting independently, CXCL10$^+$ macrophages and CD8 T_{RM}/T_{EX} subsets appear to form an interferon-driven immune niche within the TME. CXCL10$^+$, a canonical interferon-stimulated chemokine, mediates CXCR3-dependent recruitment and retention of tumor-reactive CD8 T cells, a mechanism previously linked to improved responses to PD-L1 blockade [28]. These results suggest that CXCL10$^+$ and CXCR3$^+$ cells specifically may be able to play a role in predicting response to atezolizumab + bevacizumab + SBRT. These results were similar to those observed *in vivo* in murine models and in patients with metastatic melanoma, head and neck cancer, and lung cancer following treatment with a CPI, highlighting the mechanistic overlap between tumor types [29,30].

We also did a comparative analysis on a paired sample from a single patient to determine differences in phenotypic distribution of T/NK cell subsets within the TME. When comparing the pre- and post-treatment samples, we found that T cell distribution, and CD8 T_{EX} cells were the predominant cell type pre-treatment, whereas CD8 T_{EMRA} and CD8 T_{RM} were the predominant cell type post-treatment. Examination of cytotoxic markers within the CD8 T-cell subsets showed high expression of

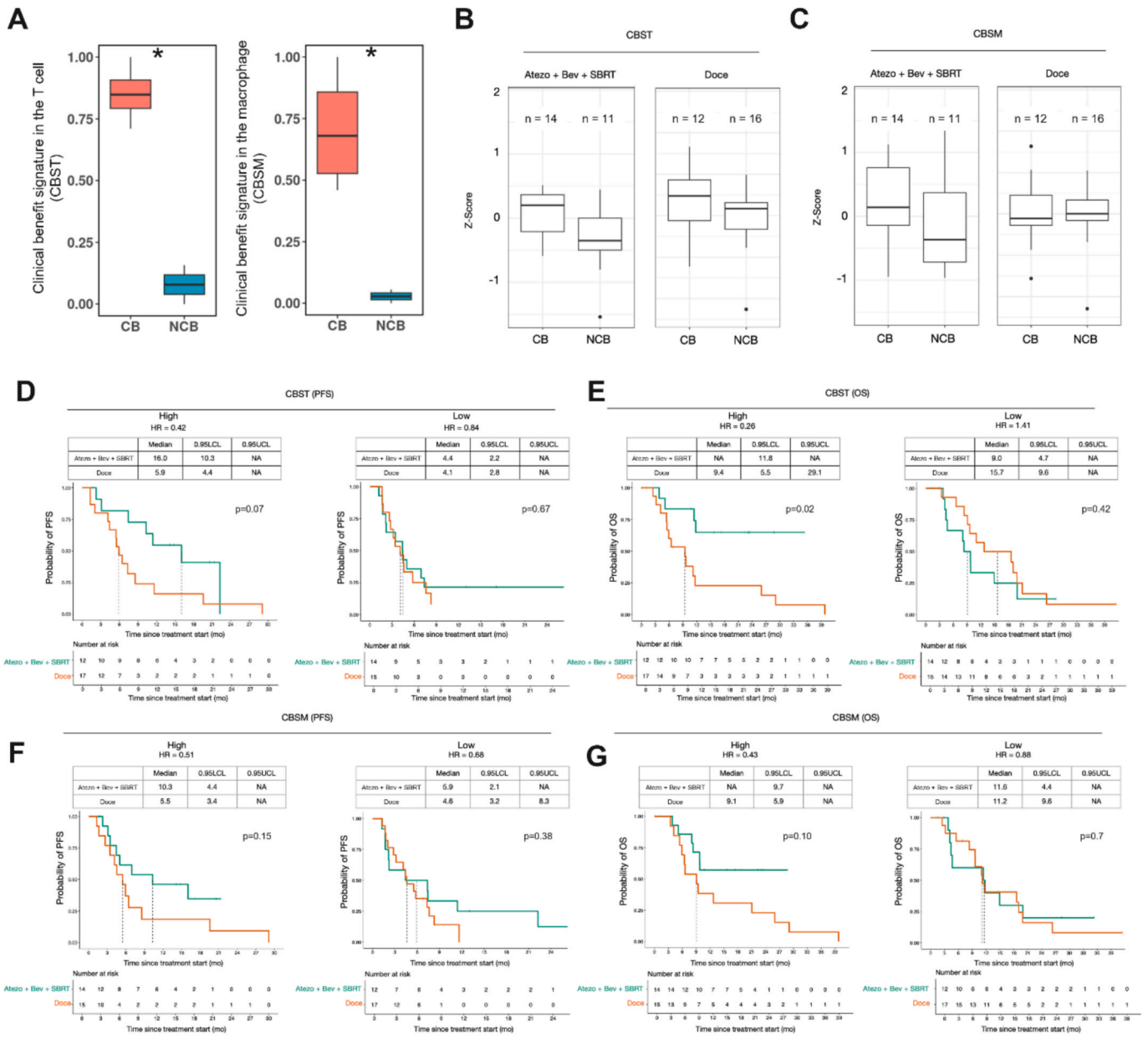

Fig. 6. Genomic correlates of clinical response to atezo + bev + SBRT. **A,** Expression of CBST and CBSM scores in scRNA-seq. Box plots show gene expression scores for response categories, with *P*-values from student *t*-tests. Boxes plus whiskers indicate the median ± IQR. The whiskers extend from either the first or third quartile to 1.5 × IQR. **B,** Expression of the CBST score in bulk RNA-seq between the CB and NCB groups in the atezo + bev + SBRT and doce arms, respectively. **C,** Expression of the CBSM score in bulk RNA-seq between the CB and NCB groups in the atezo + bev + SBRT and doce arms, respectively. **D,** Kaplan-Meier plots of PFS in bulk RNA-seq stratified by treatment arms in patients with high or low (split by median) expression score of CBST signature. **E,** Kaplan-Meier plots of OS in bulk RNA-seq stratified by treatment arms in patients with high or low (split by median) expression score of CBST signature. **F,** Kaplan-Meier plots of PFS in bulk RNA-seq stratified by treatment arms in patients with high or low (split by median) expression score of CBSM signature. **G,** Kaplan-Meier plots of OS in bulk RNA-seq stratified by treatment arms in patients with high or low (split by median) expression score of CBSM signature. atezo, atezolizumab; bev, bevacizumab; CBSM, clinical benefit signature in the macrophage; CBST, clinical benefit signature in the T cell; doce, docetaxel; IQR, interquartile range; NRPF, non-ribosome profiling; OS, overall survival; PFS, progression-free survival; RNA-seq, RNA sequencing; RPF, ribosome profiling; SBRT, stereotactic body radiation therapy.

these markers in both CD8 T_{RM} and CD8 T_{EMRA}. Moreover, genes associated with radiation response–related pathways were highly expressed in both CD8 T_{RM} and CD8 T_{EMRA}, suggesting that response to radiation therapy may be driven by interactions between these cells.

We then evaluated various subtypes of TAMs within the monocyte/macrophage compartment to identify changes in the TME pre- and post-treatment. Our findings suggest that atezolizumab + bevacizumab + SBRT response may also be influenced by the differentiation process of macrophages within the tumor seen by the increased expression of $FOLR2^+$ and $FABP4^+$ macrophages in the post-treatment sample. Our findings suggest that macrophage heterogeneity observed following combination therapy reflects distinct yet co-existing functional states within the TME. $FOLR2^+$ macrophages, previously associated with immune-supportive and vessel-associated macrophage phenotypes [31], may facilitate T cell–mediated immunity in the context of vascular normalization. In contrast, $FABP4^+$ macrophages, which are induced under hypoxic and metabolic stress conditions and correspond to lipid-associated macrophages [32], may contribute to the formation of localized immunoregulatory niches. Collectively, these observations support a unified model in which anti-angiogenic therapy and SBRT

cooperate to remodel vascular integrity, metabolic states, and interferon signaling within the TME, thereby enhancing PD-L1–directed immune reinvigoration of tumor-reactive CD8 T-cell subsets while dynamically reshaping macrophage phenotypes.

Next, we evaluated the activation of metabolic pathways in epithelial cells to identify metabolic changes in tumor cells that influence treatment response. Our analysis showed that the glycolysis score decreased, whereas the fatty acid metabolism score increased in the post-treatment sample, which suggested that bevacizumab treatment inhibited angiogenesis leading to oxygen and nutrient depletion resulting in the induction of a metabolic shift to lipid metabolism [33].

Together these results led to the identification of a curated set of T-cell– and macrophage-associated response gene signatures. The robustness of these genes was then validated with a larger study cohort. Our results suggest that increased expression of genes in these signatures within T cells and macrophages is associated with numerically improved survival outcomes in patients treated with atezolizumab + bevacizumab + SBRT vs docetaxel.

Although the gene signatures identified from bulk RNA-seq analyses were associated with survival outcomes, their current value should be viewed primarily in a translational and hypothesis-generating context. In this regard, the proposed signatures may serve as a framework for patient stratification or exploratory biomarker development in future prospective studies, as well as for generating testable hypotheses regarding mechanisms underlying treatment response or resistance. Nevertheless, independent validation across multiple cohorts and clinical contexts will be essential prior to any clinical implementation.

The results presented here require prospective validation in addition to testing in randomized clinical trials as the associations with clinical outcomes detected here are limited due to the small sample size. Furthermore, the study was limited to evaluation of TILs gene signatures and exploration of specific changes in biological pathways and did not include the inclusion of a broader set of biomarkers associated with CPI response. Although we identified potential biomarkers of response to atezolizumab + bevacizumab + SBRT, it is uncertain whether these potential biomarkers could be applied to other CPI monotherapies or combination treatments. Moreover, further studies will need to be conducted to determine practical integrations of these potential biomarkers into clinical practice.

5. Conclusions

Taken together, our results indicate that enhanced activation of T cells and macrophages may be associated with favorable clinical responses to atezolizumab + bevacizumab combined with SBRT. In particular, enrichment of CD8 T_{RM}, CD8 T_{EX}, and CXCL10^{+} macrophage populations were observed in responding tumors, suggesting that these immune features may represent candidate correlates of response in this treatment context. While the limited size and composition of the discovery cohort constrain the strength of inference, the consistent enrichment of specific immune states in responding tumors suggests that these features may warrant further evaluation in larger and independent datasets.

CRediT authorship contribution statement

Byoung Chul Cho: Writing – review & editing, Resources, Methodology, Investigation, Formal analysis, Data curation, Conceptualization. **Sun Min Lim:** Writing – review & editing, Writing – original draft, Supervision, Resources, Project administration, Methodology, Investigation, Formal analysis, Conceptualization. **Sang Hoon Lee:** Writing – review & editing, Writing – original draft, Visualization, Software, Methodology, Formal analysis, Data curation, Conceptualization. **Dong Kwon Kim:** Writing – review & editing, Writing – original draft, Visualization, Software, Methodology, Formal analysis, Data curation, Conceptualization. **Nuria Pardo:** Writing – review & editing. **Hen Prizant:** Writing – review & editing, Writing – original draft, Supervision, Project administration, Methodology, Investigation, Formal analysis, Conceptualization. **Yaacov R. Lawrence:** Writing – review & editing, Project administration, Investigation. **Nedal Al-Sakaff:** Writing – review & editing, Project administration, Data curation, Conceptualization. **Hans-Joachim Helms:** Writing – review & editing. **Velimir Gayevskiy:** Writing – review & editing, Software, Formal analysis. **Barzin Y. Nabet:** Writing – review & editing, Supervision, Resources, Project administration. **Jan Pintoffl:** Writing – review & editing, Resources, Investigation, Funding acquisition, Conceptualization. **Francois Ghiringhelli:** Writing – review & editing.

Declaration of competing interest

The authors declare the following financial interests/personal relationships which may be considered as potential competing interests: [All authors report receiving research support in the form of third-party writing assistance for this manuscript from F. Hoffmann-La Roche Ltd. B. C. Cho reports receiving research funding from AstraZeneca, Champions Oncology, CJ Bioscience, Cyrus, Dong-A ST, GI Innovation, ImmuneOnica, Janssen, J INTS Bio, Merck Sharp & Dohme, Therapex, Vertical Bio AG, and Yuhan; royalties from Champions Oncology, Crown Bioscience, Imagen, and PearlRiver Bio GmbH; consulting fees from Amgen, AnHeart Therapeutics, ArriVent, AstraZeneca, BeOne Medicines, Boehringer Ingelheim, Bristol Myers Squibb, CJ Bio, Cyrus Therapeutics, Daiichi Sankyo, Eli Lilly, Gilead, GSK, Harpoon Therapeutics, Janssen, Merck Sharp & Dohme, Novartis, Ono, Pfizer, Regeneron, Roche, Sanofi, Seagen, Takeda, and Yuhan; speakers bureau honoraria from ASCO, AstraZeneca, Guardant, Roche, ESMO, IASLC, Korean Cancer Association, Korean Society of Medical Oncology, Korean Society of Thyroid-Head and Neck Surgery, Korean Cancer Study Group, Merck Sharp & Dohme, Novartis, Pfizer, The Chinese Thoracic Oncology Society, and ZaiLab; advisory fees from Bridgebio Therapeutics, Cyrus Therapeutics, Guardant Health, J INTS Bio, KANAPH Therapeutics Inc., and Therapex Co. Ltd; other financial or nonfinancial interests with DAAN Biotherapeutics (founder), J INTS Bio (member of the board of directors), and Yonsei University Health System (employment); and is a stock owner of Bridgebio Therapeutics, Cyrus Therapeutics, Gencurix Inc., Interpark Bio Convergence Corp., J INTS Bio, and KANPH Therapeutics Inc, outside the current work. S. Lim reports receiving grants from AstraZeneca, BeOne Medicines, Boehringer Ingelheim, Daiichi Sankyo, Eli Lilly, GSK, Jiangsu Hengrui, J INTS Bio, Johnson & Johnson, Roche, Takeda, and Yuhan, outside the current work. S.H. Lee, D.K. Kim, and F. Ghiringhelli have no other disclosures to declare. N. Pardot reports receiving honoraria from F. Hoffmann-La Roche and Takeda; and travel fees from Merck Sharp & Dohme, F. Hoffmann-La Roche, Pfizer, and Takeda. H. Prizant is an employee of Genentech and stock owner of Roche, outside the current work. Y.R. Lawrence reports receiving consulting fees from F. Hoffmann-La Roche for this project; consulting fees (institution) from Zola Therapeutics Inc.; and is a stock owner of Protean Biodiagnostics. N. Al-Sakaff is an employee of F. Hoffmann-La Roche and stock owner of Roche, outside the current work. H.-J. Helms is an employee of F. Hoffmann-La Roche and stock owner of Roche, outside the current work. V. Gayevskiy is a contractor for Genentech and an employee of Rancho BioSciences, outside the current work. B. Nabet is an employee of Genentech and stock owner of Roche, outside the current work. J. Pintoffl is an employee and stock owner of Roche, outside the current work].

Acknowledgments

F. Hoffmann-La Roche Ltd. sponsored this study and was involved in the study design, collection, analysis, and interpretation of data, as well as the writing of the report. Authors had full access to all data, and the corresponding author had final responsibility for the decision to submit the results for publication.

The authors thank the patients who participated in the trial, and their families. We also thank the clinical study site investigators and site personnel. Medical writing assistance for this manuscript was provided by Nimisha H. Bhoola, PhD, of Nucleus Global, an Inizio Company, and funded by F. Hoffmann-La Roche Ltd.

Appendix A. Supplementary data

Supplementary data to this article can be found online at https://doi.org/10.1016/j.lungcan.2026.109354.

References

[1] T. Lu, X. Yang, Y. Huang, M. Zhao, M. Li, K. Ma, et al., Trends in the incidence, treatment, and survival of patients with lung cancer in the last four decades, Cancer Manag. Res. 11 (2019) 943–953.
[2] Y. Wang, K. Kondrat, J. Adhikari, Q. Nguyen, Q. Yu, D. Uprety, Survival trends among patients with metastatic non-small cell lung cancer before and after the approval of immunotherapy in the United States: a surveillance, epidemiology, and end results database-based study, Cancer 131 (1) (2025) e35476.
[3] L.E. Hendriks, K.M. Kerr, J. Menis, T.S. Mok, U. Nestle, A. Passaro, et al., Non-oncogene-addicted metastatic non-small-cell lung cancer: ESMO Clinical Practice Guideline for diagnosis, treatment and follow-up, Ann. Oncol. 34 (4) (2023) 358–376.
[4] A. Insa, P. Martin-Martorell, R. Di Liello, M. Fasano, G. Martini, S. Napolitano, et al., Which treatment after first line therapy in NSCLC patients without genetic alterations in the era of immunotherapy? Crit. Rev. Oncol. Hematol. 169 (2022) 103538.
[5] G. Francois, R.L. Yaacov, F. Enriqueta, Z. Alona, G. Laurent, G. Alastair, et al., Atezolizumab and bevacizumab, with or without radiotherapy, versus docetaxel in patients with metastatic non-small cell lung cancer previously treated with a checkpoint inhibitor and chemotherapy: results from the randomized, phase Ib/II MORPHEUS-Lung study, J. Immunother. Cancer 13 (8) (2025) e011892.
[6] R.K. Jain, Normalizing tumor vasculature with anti-angiogenic therapy: a new paradigm for combination therapy, Nat. Med. 7 (9) (2001) 987–989.
[7] O.E. Rahma, F.S. Hodi, The intersection between tumor angiogenesis and immune suppression, Clin. Cancer Res. 25 (18) (2019) 5449–5457.
[8] J.J. Wallin, J.C. Bendell, R. Funke, M. Sznol, K. Korski, S. Jones, et al., Atezolizumab in combination with bevacizumab enhances antigen-specific T-cell migration in metastatic renal cell carcinoma, Nat. Commun. 7 (2016) 12624.
[9] A.L. Cheng, S. Qin, M. Ikeda, P.R. Galle, M. Ducreux, T.Y. Kim, et al., Updated efficacy and safety data from IMbrave150: atezolizumab plus bevacizumab vs. sorafenib for unresectable hepatocellular carcinoma, J. Hepatol. 76 (4) (2022) 862–873.
[10] M. Provencio, A.L. Ortega, J. Coves-Sarto, V. Calvo, R. Marse-Fabregat, M. Domine, et al., Atezolizumab plus bevacizumab as first-line treatment for patients with metastatic nonsquamous non-small cell lung cancer with high tumor mutation burden: a nonrandomized controlled trial, JAMA Oncol. 9 (3) (2023) 344–353.
[11] C.T. Garnett, C. Palena, M. Chakraborty, K.Y. Tsang, J. Schlom, J.W. Hodge, Sublethal irradiation of human tumor cells modulates phenotype resulting in enhanced killing by cytotoxic T lymphocytes, Cancer Res. 64 (21) (2004) 7985–7994.
[12] S. Wan, S. Pestka, R.G. Jubin, Y.L. Lyu, Y.C. Tsai, L.F. Liu, Chemotherapeutics and radiation stimulate MHC class I expression through elevated interferon-beta signaling in breast cancer cells, PLoS One 7 (3) (2012) e32542.
[13] H. Menon, R. Ramapriyan, T.R. Cushman, V. Verma, H.H. Kim, J.E. Schoenhals, et al., Role of radiation therapy in modulation of the tumor stroma and microenvironment, Front. Immunol. 10 (2019) 193.
[14] W. Ngwa, O.C. Irabor, J.D. Schoenfeld, J. Hesser, S. Demaria, S.C. Formenti, Using immunotherapy to boost the abscopal effect, Nat. Rev. Cancer 18 (5) (2018) 313–322.
[15] W. Theelen, H.M.U. Peulen, F. Lalezari, V. van der Noort, J.F. de Vries, J. Aerts, et al., Effect of pembrolizumab after stereotactic body radiotherapy vs pembrolizumab alone on tumor response in patients with advanced non-small cell lung cancer: results of the PEMBRO-RT phase 2 randomized clinical trial, JAMA Oncol. 5 (9) (2019) 1276–1282.
[16] J.N. Bodor, Y. Boumber, H. Borghaei, Biomarkers for immune checkpoint inhibition in non-small cell lung cancer (NSCLC), Cancer 126 (2) (2020) 260–270.
[17] A.K. Bryant, K. Sankar, G.W. Strohbehn, L. Zhao, V. Daniel, D. Elliott, et al., Prognostic and predictive role of PD-L1 expression in stage III non-small cell lung cancer treated with definitive chemoradiation and adjuvant durvalumab, Int. J. Radiat. Oncol. Biol. Phys. 113 (4) (2022) 752–758.
[18] Y. Liu, D. Qin, J. Fu, T lymphocyte heterogeneity in NSCLC: implications for biomarker development and therapeutic innovation, Front. Immunol. 16 (2025) 1604310.
[19] I. Gataa, L. Mezquita, C. Rossoni, E. Auclin, M. Kossai, F. Aboubakar, et al., Tumour-infiltrating lymphocyte density is associated with favourable outcome in patients with advanced non-small cell lung cancer treated with immunotherapy, Eur. J. Cancer 145 (2021) 221–229.
[20] V.K. Anagnostou, J.R. Brahmer, Cancer immunotherapy: a future paradigm shift in the treatment of non-small cell lung cancer, Clin. Cancer Res. 21 (5) (2015) 976–984.
[21] F. Li, C. Li, X. Cai, Z. Xie, L. Zhou, B. Cheng, et al., The association between CD8+ tumor-infiltrating lymphocytes and the clinical outcome of cancer immunotherapy: a systematic review and meta-analysis, EClinicalMedicine 41 (2021) 101134.
[22] Y. Geng, Y. Shao, W. He, W. Hu, Y. Xu, J. Chen, et al., Prognostic role of tumor-infiltrating lymphocytes in lung cancer: a meta-analysis, Cell. Physiol. Biochem. 37 (4) (2015) 1560–1571.
[23] B. Liu, X. Hu, K. Feng, R. Gao, Z. Xue, S. Zhang, et al., Temporal single-cell tracing reveals clonal revival and expansion of precursor exhausted T cells during anti-PD-1 therapy in lung cancer, Nat Cancer. 3 (1) (2022) 108–121.
[24] F. Djenidi, J. Adam, A. Goubar, A. Durgeau, G. Meurice, V. de Montpreville, et al., CD8+CD103+ tumor-infiltrating lymphocytes are tumor-specific tissue-resident memory T cells and a prognostic factor for survival in lung cancer patients, J. Immunol. 194 (7) (2015) 3475–3486.
[25] S. Corgnac, I. Malenica, L. Mezquita, E. Auclin, E. Voilin, J. Kacher, et al., CD103(+)CD8(+) T(RM) cells accumulate in tumors of anti-PD-1-responder lung cancer patients and are tumor-reactive lymphocytes enriched with Tc17, Cell Rep. Med. 1 (7) (2020) 100127.
[26] C.L. Hsu, D.L. Ou, L.Y. Bai, C.W. Chen, L. Lin, S.F. Huang, et al., Exploring markers of exhausted CD8 T cells to predict response to immune checkpoint inhibitor therapy for hepatocellular carcinoma, Liver Cancer. 10 (4) (2021) 346–359.
[27] J.P. Guegan, F. Peyraud, B. Dadone-Montaudie, D. Teyssonneau, L.J. Palmieri, E. Clot, et al., Analysis of PD1, LAG3, TIGIT, and TIM3 expression in human lung adenocarcinoma reveals a 25-gene signature predicting immunotherapy response, Cell Rep. Med. 5 (12) (2024) 101831.
[28] S. Cappuyns, G. Philips, V. Vandecaveye, B. Boeckx, R. Schepers, T. Van Brussel, et al., PD-1(-) CD45RA(+) effector-memory CD8 T cells and CXCL10(+) macrophages are associated with response to atezolizumab plus bevacizumab in advanced hepatocellular carcinoma, Nat. Commun. 14 (1) (2023) 7825.
[29] I.G. House, P. Savas, J. Lai, A.X.Y. Chen, A.J. Oliver, Z.L. Teo, et al., Macrophage-derived CXCL9 and CXCL10 are required for antitumor immune responses following immune checkpoint blockade, Clin. Cancer Res. 26 (2) (2020) 487–504.
[30] M.T. Chow, A.J. Ozga, R.L. Servis, D.T. Frederick, J.A. Lo, D.E. Fisher, et al., Intratumoral activity of the CXCR3 chemokine system is required for the efficacy of anti-PD-1 therapy, Immunity 50 (6) (2019) 1498–512 e5.
[31] Y. Komohara, D. Kurotaki, H. Tsukamoto, Y. Miyasato, H. Yano, C. Pan, et al., Involvement of protumor macrophages in breast cancer progression and characterization of macrophage phenotypes, Cancer Sci. 114 (6) (2023) 2220–2229.
[32] D. Zhang, M. Wang, G. Liu, X. Li, W. Yu, Z. Hui, et al., Novel FABP4(+)C1q(+) macrophages enhance antitumor immunity and associated with response to neoadjuvant pembrolizumab and chemotherapy in NSCLC via AMPK/JAK/STAT axis, Cell Death Dis. 15 (10) (2024) 717.
[33] J. Wang, J. Millstein, Y. Yang, S. Stintzing, H. Arai, F. Battaglin, et al., Impact of genetic variants involved in the lipid metabolism pathway on progression free survival in patients receiving bevacizumab-based chemotherapy in metastatic colorectal cancer: a retrospective analysis of FIRE-3 and MAVERICC trials, EClinicalMedicine 57 (2023) 101827.